Chapter

New Robust Control Design of Brake-by-Wire Actuators

Ehsan Arasteh and Francis Assadian

Abstract

This chapter discusses control design of three different brake-by-wire actuators. The brakes studied include an Electro-Hydraulic brake with pressure modulation for wheel slip control, and two different Electro-Mechanical Brake configurations that directly use electric motors to control the movement of the caliper for wheel slip control. After modeling the actuators with the use of bond graphs, a cascaded control architecture is used to control these active systems. Individual controllers are designed using Youla robust control design method. Then, a feed-forward disturbance rejection is designed and added to the loops and its effectiveness is analyzed. Finally, a one-wheel model is used to compare these brake-by-wire systems in terms of stopping distance and actuator efforts.

Keywords: brake-by-wire, electro-hydraulic brake, robust control, electro-mechanical brake, disturbance rejection

1. Introduction

X-By-Wire technologies are the future of the automotive industry due to an increasing demand for electrification and fuel efficiency. Their electronic architectures and interface also make them a great candidate for autonomous and hybrid electric/electric vehicles. Among all the necessary by-wire technologies, brake-by-wire systems are a priority due to their safety-critical nature role in the vehicle [1, 2].

Brake-by-wire systems can reduce component weight and allow the actuators to consume energy only when required by blending both regenerative braking and friction braking. This can minimize fuel consumption and CO2 emissions. Using sensors and control methods, caliper drag can be eliminated by making brake-by-wire technology even more energy efficient. Individual wheel braking and faster activation time can be combined with the vehicle's ECS system to make the vehicle safer. The reliability of new actuators and the risk and cost associated with deploying new brake technologies are the main hurdles of brake-by-wire systems becoming a popular choice for the automotive manufacturers [3, 4].

Brake systems are categorized into wet and dry brakes. Wet brakes employ fluids for their operation, and dry brakes are usually purely mechanical systems. Electro-hydraulic brake systems are a type of wet brakes where their pressure is modified using pressure modulators that can be controlled electronically. The pressure source can be packaged in one centralized location for all four wheels like Bosch's first electro-hydraulic brake system [5], or it can be local to each wheel like

MKC-l from Continental [6] (local Electro-hydraulic brakes). Dry brakes can also be realized in a few different configurations. There is an electro-mechanical brake that utilizes a small motor, planetary gear set and a roller-screw to move the brake pad [7–13]. However, this type of brake requires a 42 Volt motor to operate and consumes a lot of energy [3]. Electronic-wedge brakes on the other hand, uses a wedge mechanism to create a system that draws the wedge pad inside the brake; therefore, requiring less energy to operate [13–21]. Vienna Engineering also came up with a similar idea that uses a crank-shaft mechanism that reduces the complexity of reduction gears and roller screws [22–25].

Purely dry brakes such as Electronic Wedge and VE brakes, are going to be costlier that Electro-Hydraulic brakes since they are newer technologies and require more research and development to productionize. On the other hand, EHB has already been in the market for a while. The other challenge for purly dry brakes is reliability since they have more electronic components and they all need to reliably perform in a harsh environment near the brake where vibration, shock and high temperatures can have significant impact [3].

In this work, we have chosen to study Electro-Hydraulic (EHB), Electro-Mechanical (EMB) and Electronic Wedge Brakes (EWB). We will start by modeling the brakes using bond graph in Section 2. Bond graph is graphical representation method to model dynamical systems that utilizes flow of energy. It is an easy and intuitive way to model physical systems especially the ones that are in the multi-energy domain (e.g. Electro-Mechanical, Electro-Hydraulic). Readers can take a look at [26] for further readings on bond graphs.

After modeling the actuators, we will design the controllers using Youla Paramerization technique. Finally, we will add disturbance rejection and compare results for EMB and EWB controllers and show their effectiveness. The purpose of this book chapter is to show the process of modeling of three different brake-by-wire actuators and designing their robust controllers using Youla paramerization.

2. System modeling

In this section, we discuss the schematics, bond graphs, and the equations of motion based on the bond graphs for each brake system. All the actuator models include a one-wheel vehicle model that is represented in **Figure 1**. It includes a moving wheel with a rotational inertia connected to a point mass. This simple dynamic model is very useful for preliminary studies of brake actuators and algorithms (such as ABS and TCS) and is easy to implement on the test rig. This simple

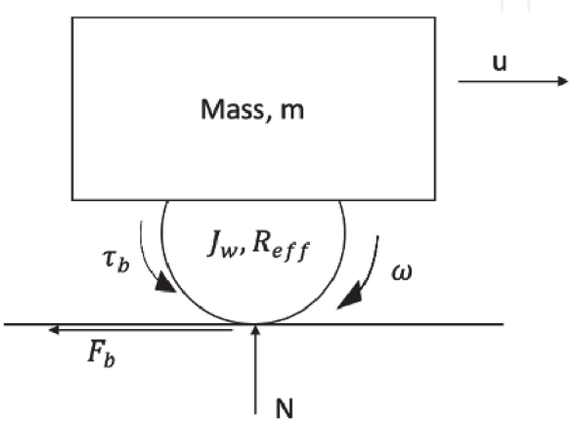

Figure 1.
One-wheel vehicle model used to analyze the brake actuator behaviors.

model is only utilized to study longitudinal dynamic effects in the vehicle. This model suffices for studying most of the brake-by-wire actuators and ABS technologies since it focuses on the longitudinal dynamics of the vehicle. Higher fidelity vehicle models, which include lateral dynamics, such as bicycle model and extended bicycle model will be considered in the future, once the preliminary comparisons of different actuators are studied and revealed using this simple model [25, 27–30]. The bond graph of this model is included in **Figure 2**.

State equations for this model are as follows

$$\dot{p}_{\omega} = J_w \dot{\omega} = F_b R_{eff} - \tau_b - B\omega \tag{1}$$

$$\dot{p}_u = m\dot{u} = -F_b \tag{2}$$

Where u is forward velocity, ω is wheel angular velocity, τ_b is braking torque, F_b is braking force, N is normal force, B is bearing friction coefficient, R_{eff} is effective wheel radius, p_{ω} is the angular momentum of the wheel, and p_u is the vehicle's momentum. For the braking force modeling, the Burckhardt tire model is chosen in which the coefficient of friction (μ) is a function of the longitudinal slip (λ) (Eq. 4) and the longitudinal slip is defined in Eq. 3 [31, 32].

$$\lambda = \frac{u - \omega R_{eff}}{|u|} \tag{3}$$

$$F_b = \mu(\lambda) \cdot N = \left[c_1\left(1 - e^{-c_2\lambda}\right) - c_3\lambda\right] \cdot N \tag{4}$$

where N is the normal force. The state equations describing the one-wheel model will always be present in all brake type models since the vehicle model will stay the same.

2.1 Electro-hydraulic brake actuator

The schematic of an electro-hydraulic brake (EHB) actuator is presented in **Figure 3**. It includes a hydraulic pipe which carries the hydraulic fluid with the pressure input (P_{in}) to a cylinder chamber, which in turn changes this pressure into the movement of the brake pad. Therefore, the brake pad movement results in stopping the brake disk from moving [33].

The bond graph model is derived based on the schematic in **Figure 3**. The input is modulated pressure, and this pressure is an input to the hydraulic line, where, by using a transformer, it results in the brake pad movement (the pressure reservoir and the motor that modulates the pressure are not included in the model and will be added in the future studies). The interaction between the brake pad and the wheel is modeled with a stiffness (k_{cal}). Brake torque is also modeled by a modulated resistance which changes with the displacement of the brake pad.

State equations (Eq. 5–8) are derived based on the bond graph in **Figure 4**.

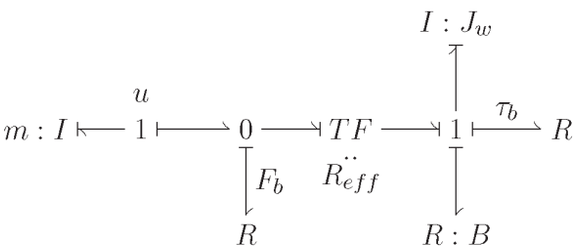

Figure 2.
One-wheel bond graph.

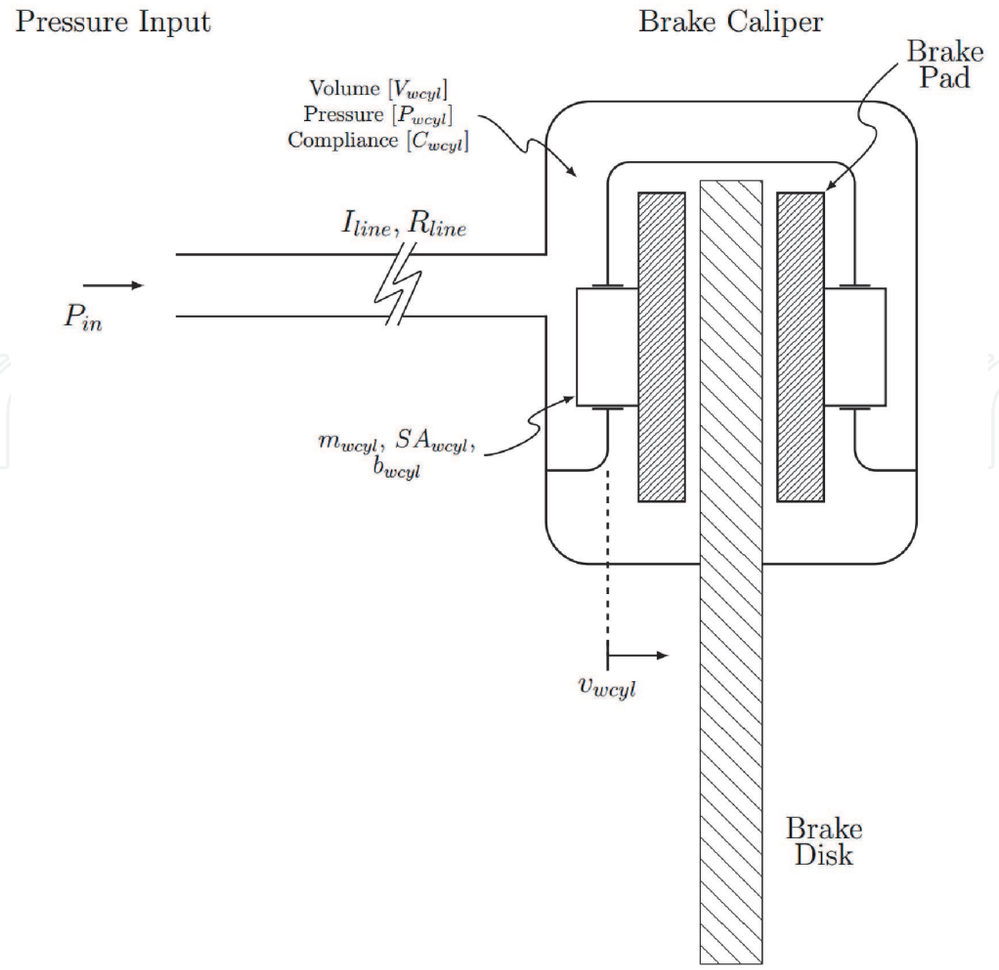

Figure 3.
Electro-hydraulic brake actuator (EHB) schematics [33].

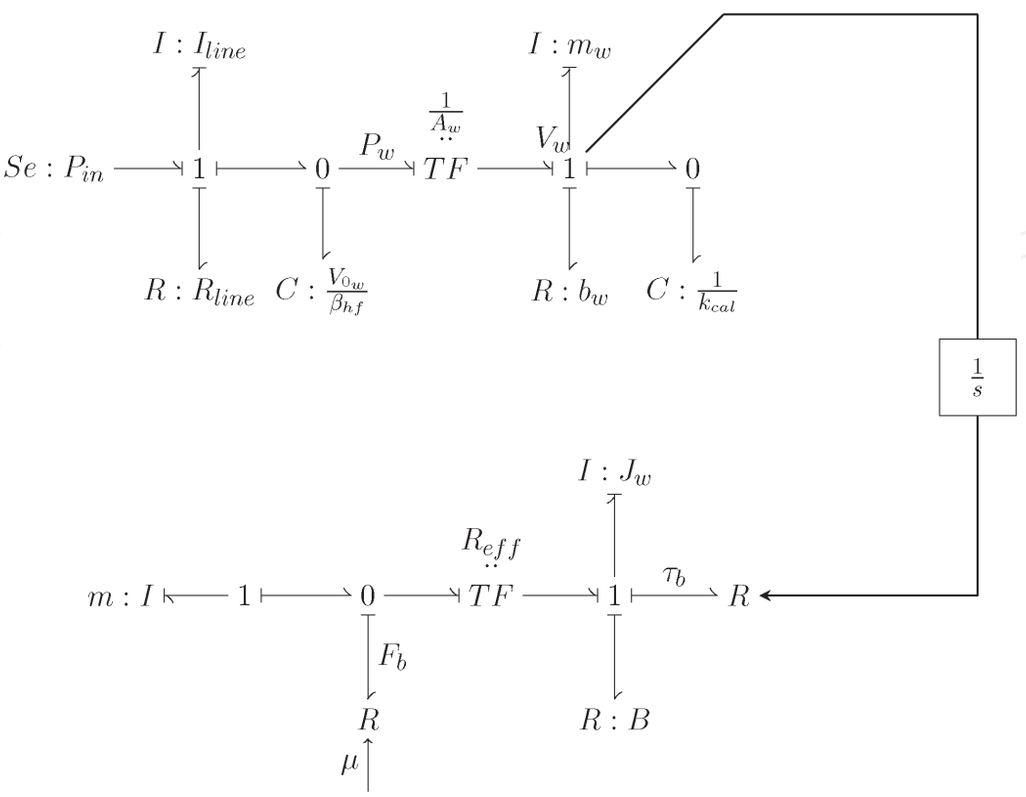

Figure 4.
EHB bond graph.

$$\dot{p}_{line} = P_{in} - R_{line}\frac{p_{line}}{I_{line}} - q_w\frac{\beta_h f}{V_{0_w}} \tag{5}$$

$$\dot{q}_w = \frac{p_{\text{line}}}{I_{\text{line}}} - A_w\frac{p_w}{m_w} \tag{6}$$

$$\dot{p}_w = A_w q_w\frac{\beta_{hf}}{V_{0_w}} - b_w\frac{p_w}{m_w} - q_{cal}k_{cal} \tag{7}$$

$$\dot{q}_{cal} = \frac{p_w}{m_w} \tag{8}$$

Where $R_{line}, p_{line}, I_{line}, \beta_{hf}, V_{0_w}, A_w, p_w, V_w$, and q_{cal} are hydraulic line resistance, hydraulic line pressure, line inertia, bulk modulus, volume of cylinder chamber, surface area of the piston, pressure on the brake pad, velocity of the brake pad, and brake pad position, respectively. The brake torque is calculated using Eq. 9.

$$\tau_b = \begin{cases} 2\mu_{cal}r_{eff}k_{cal}(x_{cal} - x_0) \ , & \text{if } x_{cal} \geq x_0 \\ 0, & \text{otherwise} \end{cases} \tag{9}$$

Where $\mu_{cal}, r_{eff}, x_{cal}$, and x_0 are brake friction coefficient between the pad and the wheel, brake pad effective radius, brake pad position (same as q_{cal}), and brake clearance, respectively. Eqs. 5–9 along with Eqs. 1–4 present the state equations for this brake system [29].

2.2 Electro-mechanical brake actuator

Figure 5 shows a schematic of an electro-mechanical brake actuator. It consists of an electric motor, planetary gear set, ball screw, piston, brake pad, and floating caliper to oppose the brake pad. In this actuator, the motor's rotational motion becomes the brake pad's movement through one (or more) planetary gear sets and a ball screw mechanism. This movement will then create a clamp force given by F_{cl} in **Figure 5** [10, 34].

Figure 6 illustrates the bond graph model for an electro-mechanical brake actuator (EMB). The input to the system is voltage (V_{in}) to the motor. The motor includes an inductance (L_m) and a resistance (R_m). The motor's current is proportional to a torque on the shaft and this proportionality is modeled by a gyrator (with K_t representing the motor constant). The shaft has a rotational inertia (J_m). The resistance that exists inside the planetary gear set, the ball-screw mechanism and the motor shaft is lumped together and modeled by an R-element. This resistance element is explained more in the next section.

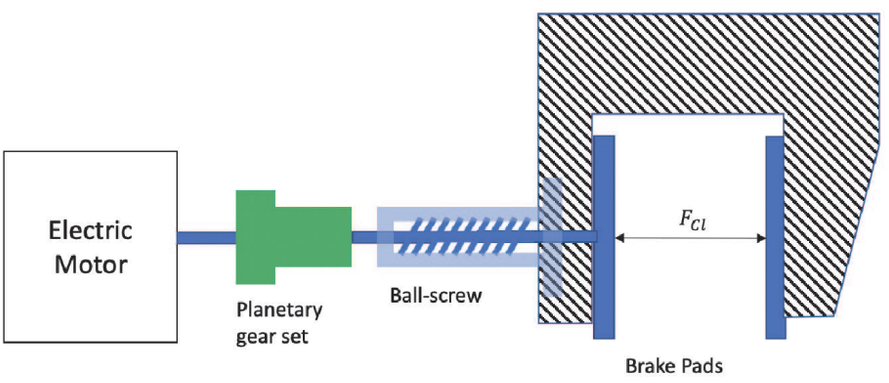

Figure 5.
EMB Schematics (adapted from [34, 35]).

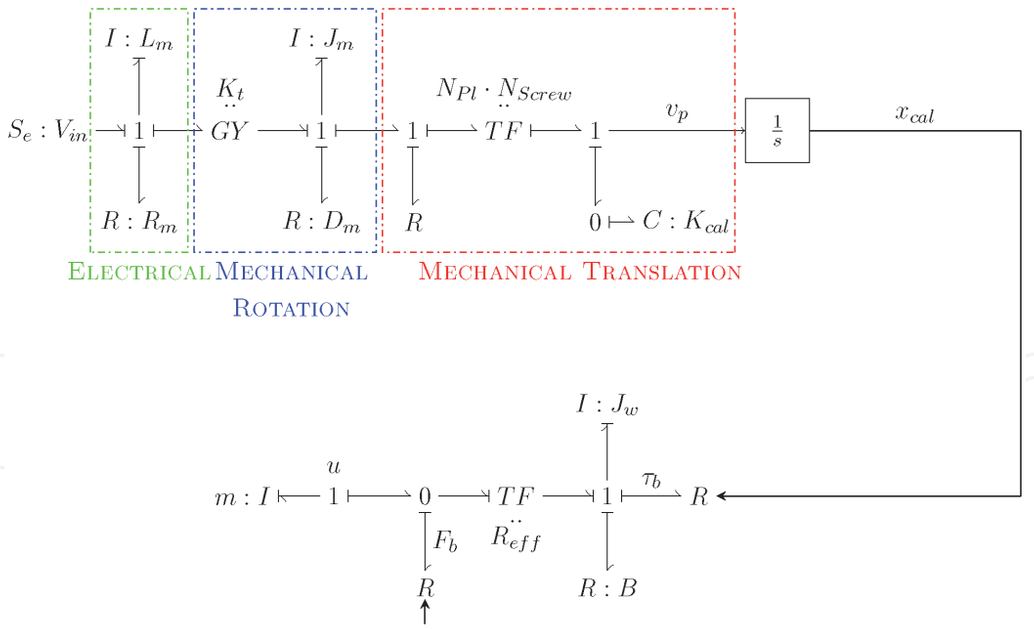

Figure 6.
EMB's bond graph.

The transformer is then used for the planetary gear set ratio (N_{pl}) and the ball-screw mechanism lead ratio (N_{Screw}). And finally, the interaction between the brake pad and the wheel is modeled with a stiffness similar to the one in the electro-hydraulic brake system's bond graph (K_{cal}).

Based on the bond graph in **Figure 6**, the state equations are presented in Eqs. 10–12. Also, the brake torque is calculated similar to the EHB actuator using Eq. 9.

$$\dot{I}_m = \frac{1}{L_m}\left(V_{in} - R_m \cdot I_m - K_t \cdot \omega_m\right) \tag{10}$$

$$\dot{\omega}_m = \frac{1}{J_m}\left(K_t \cdot I_m - D_m \cdot \omega_m - \tau_f - N_p \cdot N_s \cdot K_{cal} \cdot max\left(x_{cal} - x_0, 0\right)\right) \tag{11}$$

$$\dot{X}_{cal} = N_s \cdot N_p \cdot \omega_m \tag{12}$$

The lumped friction torque (τ_f) is modeled using Karnopp friction with the Coulomb friction torque (τ_c) and maximum stiction torque (τ_s) having an affine relationship with the clamp force (F_{cl}). The area around zero of the motor rotational velocity is given by $d\omega$, and ω_m is the motor's rotational velocity and τ_{pl_0} is the friction torque when the shaft is not moving. C and G are constants that can be acquired using experimental results [10, 36].

$$\tau_f = \begin{cases} \tau_c \cdot \text{sign}(\omega_m) + b_v \cdot \omega_m & |\omega_m| \geq \text{d}\omega \\ \min\left(\left|\tau_{pl_0}\right|, \ \tau_s\right|\left|\right) \cdot \text{sign}\left(\tau_{pl_0}\right) & \text{else} \end{cases} \tag{13}$$

$$\tau_c = C + G \cdot F_{cl} \tag{14}$$

2.3 Electronic wedge brake actuator

We can draw the schematic for the wedge and the caliper in **Figure 7**. The motor's rotational velocity is being translated through a planetary gear set (not shown in the schematic) and a roller screw to a linear force on the wedge. Motor

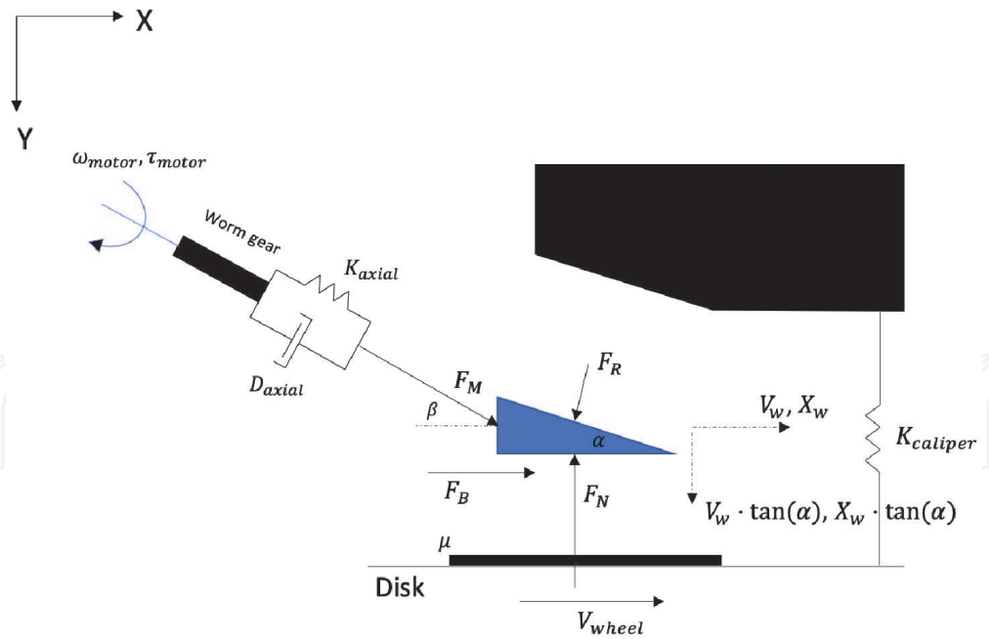

Figure 7.
EWB schematics.

shaft's axial stiffness and resistance is also added to the system. $K_{caliper}$ represents the stiffness of the caliper itself the stiffness between the wedge and the disk.

If we write the force equations for the wedge brake, we can get X-direction:

$$m_w \dot{V}_w = F_M \cos\beta + F_B - F_R \sin\alpha \tag{15}$$

Y-direction:

$$m_w \dot{V}_w \tan(\alpha) = F_M \sin\beta - F_N + F_R \cos\alpha \tag{16}$$

And for the disk surface, we can write

$$F_N = K_{\mathrm{Ca1}} \cdot X_w \tan(\alpha) \tag{17}$$

By rearranging Eqs. 15–17, we can remove the reaction force in the equations and write Eq. 18. We have incorporated Eq. 18 into the bond graph using 3 transformers.

$$\dot{V}_{\mathrm{W}} = \frac{1}{m_W(1+\tan^2\alpha)}\left(\frac{1}{\cos\alpha}F_M + (\mu_{cal} - \tan\alpha)\tan\alpha(K_{cal}) \cdot X_w\right) \tag{18}$$

Figure 8 represents the bond graph of the electronic wedge brake. The input to the system is motor voltage. The electric motor section remains the same as discussed in the previous sections. The transformer includes the roller-screw's lead ratio $\left(\frac{L}{2\pi}\right)$ and the planetary gear set's gear ratio (N). For the sake of simplicity, we assume, $\alpha = \beta$. F_B is the brake force that can be calculated from the relative velocity between the caliper and the wheel; however, since the wheel's velocity is much faster than the caliper's velocity, for the sake of simplicity, we assume that it would only be a function of caliper's movement. Finally, the transformer gains Tl, T2, and T3, based on Eq. 18, will become Eqs. 19–21.

$$T_1 = \frac{1}{\cos\alpha} \cdot \frac{1}{1+\tan^2\alpha} = cos(\alpha) \tag{19}$$

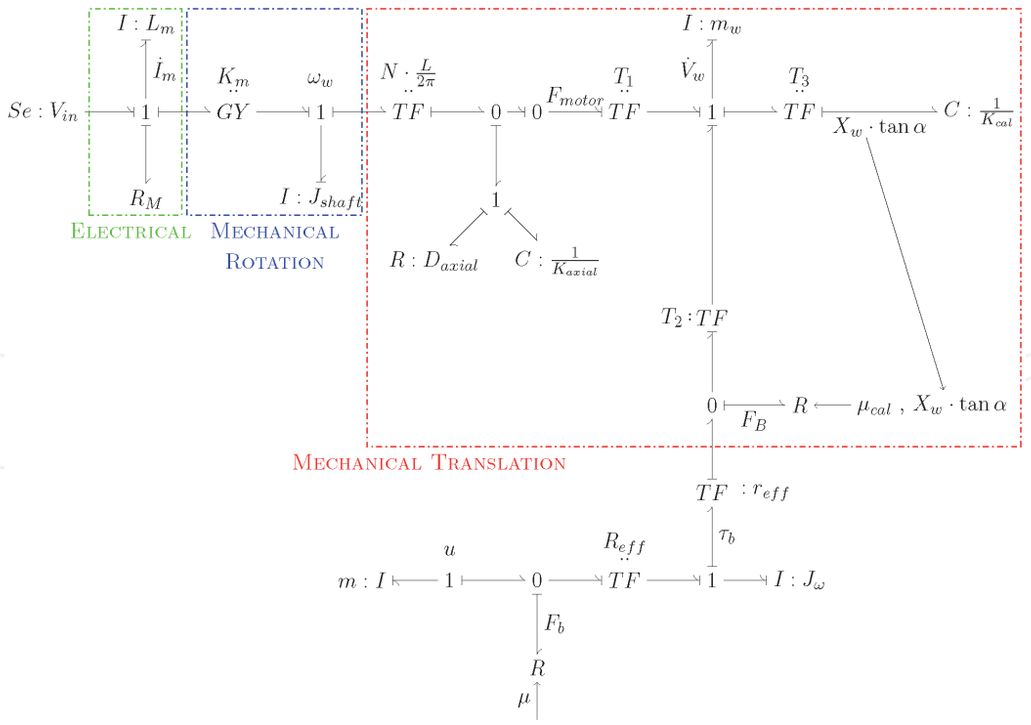

Figure 8.
EWB's Bond Graph.

$$T_2 = \frac{1}{1 + \tan^2\alpha} \tag{20}$$

$$T_3 = \frac{\tan\alpha}{1 + \tan^2\alpha} \tag{21}$$

Based on the bond graph, the equations of motion for the wedge brake are provided by Eqs. 22–28. Brake Torque is also calculated the same as other actuators.

$$\dot{i}_m = \frac{1}{L_m}(V_{in} - i_m \cdot R_m - K_m \cdot \omega_m) \tag{22}$$

$$\dot{q}_{ax} = LN\omega - \frac{V_w}{cos\,(\alpha)} \tag{23}$$

$$F_m = K_{ax} q_{ax} + D_{ax}\dot{q}_{ax} \tag{24}$$

$$\dot{\omega} = \frac{1}{J_m}\{K_m i_m - D_m \cdot \omega - L \cdot N \cdot F_m\} \tag{25}$$

$$\dot{V}_w = \frac{1}{M_w(1 + tan^2(\alpha))}\{\frac{F_m}{cos\,(\alpha)} + (K_{cal} \cdot X_w \cdot tan\,(\alpha)(\mu_{cal} - tan\,(\alpha))\} \tag{26}$$

$$\dot{X}_w = V_w \tag{27}$$

$$F_b = \mu_{cal} K_{cal} X_w\, tan\,(\alpha) \tag{28}$$

3. Control strategy

In this section, we discuss the control strategy for each brake actuator. For each of the brake actuators, a transfer function is obtained using the linearized equations of motion provided in the previous sections (all the nonlinearities in the frictions and caliper stiffness are linearized). Controllers in each case are designed using Youla-Kucera parameterization, which we will discuss in details in this section. This

control strategy ensures internal stability, robustness, and reference tracking of the closed-loop system.

In the electro-hydraulic brake actuator, the pressure is the input and the output is brake force $\left(G_p = \frac{F_b}{P_{in}}\right)$. A controller was designed around the plant to follow a specific brake reference force. In practice, we would need to either estimate the brake force (or brake torque) or use a sensor to acquire that information [29]. For the electro-mechanical and electronic-wedge brakes, a cascaded control scheme is used. The schematics of these control architectures are shown in **Figures 9** and **10** [8, 10]. In the cascaded control scheme, each inner closed-loop system is a new plant for the outer loop controller design. In this case, for the first loop, the input is the motor's voltage and the output is the motor's current. For the second loop, the input is the motor's current and the output is the motor's angular velocity. Lastly, for the most outer loop, the input is the motor's angular velocity and the output is clamping force (the normal force that clamps the wheel). Cascaded control increase performance and robustness of systems with relatively more nonlinearities. Hence, the controllers for the EMB and EWB were designed using cascaded control since they have more nonlinearities (e.g. mechanical friction) than the standard EHB. The current and angular velocity of the shaft can be directly measured while the clamp force requires to either be estimated or measured using a force sensor. Additionally, each loop has a disturbance which we will ignore in the first part of the control design. Later, we will use a disturbance rejection scheme to migitage the effect of these disturbances.

3.1 Robust control design using Youla parameterization

Youla parameterization is a robust control technique that allows for shaping the desired closed-loop transfer function (T), known as complimentary sensitivity transfer function, while ensuring internal stability, disturbance rejection at low frequency, and sensor noise and unmodeled disturbance rejections at high frequencies. The main

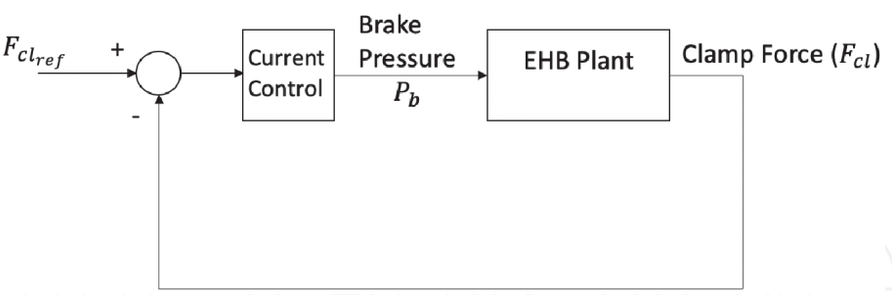

Figure 9.
Overall control architecture of EHB actuator.

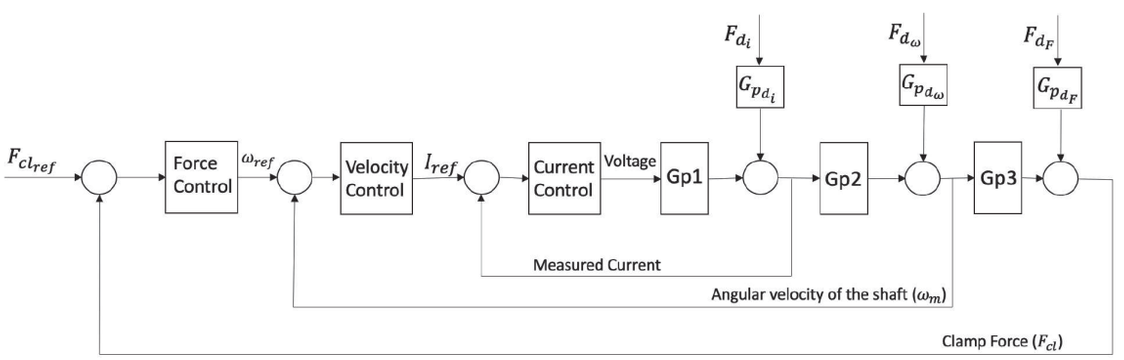

Figure 10.
Overall control architecture of EMB and EWB actuators.

idea is to shape the closed-loop transfer function (T) with a transfer function called Youla (Y(s)), which when multiplied by the plant transfer function (G_p) would become the closed loop transfer function (Eq. 29). To have a good tracking performance at steady-state, T(s) should be one in magnitude at low frequencies, it should be small in magnitude at high frequencies to ensure high frequency disturbance rejection.

$$T(s) = G_p(s) \cdot Y(s) \tag{29}$$

Therefore, according to Eq. 29, we can shape the closed-loop transfer function (provided that we meet the interpolation conditions, for ensuring internal stability, mentioned below). It is worth noting that Youla transfer function is related to the actuator effort so having a low magnitude Youla especially at high frequencies would keep the actuator effort low.

The closed loop transfer function (T(s)) is complementary to the sensitivity transfer function (S(s)) and the vector sum of these two transfer functions as given by (Eq. 30) is known as algebraic constraint. Therefore, this sensitivity transfer function should be small at low frequencies (to reject low frequency disturbances) and equal to one in magnitude at high frequencies due to the algebraic constraint.

$$S(s) = 1 - T(s) \tag{30}$$

If G_p is stable, the feedback loop would be internally stable if and only if Y(s) is selected to be stable. When G_p is not stable, $Y(s)$, $S(s)$, $T(s)$, and G_pS must all be stable to make the feedback loop internally stable. Therefore, to meet these conditions if there is an unstable pole (α_p) repeated n times in the plant (G_p), Eqs. 31 and 32, which are the interpolation conditions, have to be met (If the unstable pole is not repeated, Eq. 31 would suffice to meet the interpolation conditions).

$$T(\alpha_p) = 1, \;\; S(\alpha_p) = 0 \tag{31}$$

$$\frac{d^k T}{ds^k}(\alpha_p) = 0, \;\; \frac{d^k S}{ds^k}(\alpha_p) = 0, \qquad For \qquad 1 \le k \le n \tag{32}$$

For a non-minimum phase zero (α_z) repeated n time, zeros in the RHP (Right Half Plane), the interpolation conditions are given by Eqs. 33 and 34. If the unstable zero is not repeated, Eq. 33 is the only interpolation condition that has to be met [37].

$$S(\alpha_z) = 1, \;\; T(\alpha_z) = 0 \tag{33}$$

$$\frac{d^k S}{ds^k}(\alpha_z) = 0, \;\; \frac{d^k T}{ds^k}(\alpha_z) = 0, \qquad For \qquad 1 \le k \le n \tag{34}$$

If all the conditions above are met, then we can obtain the controller using Eq. 35.

$$G_c(s) = Y(s) \cdot S(s)^{-1} \tag{35}$$

In the following subsections, we discuss the controller design for the proposed brake actuators using the above strategy known as Youla parameterization.

3.2 EHB Youla control design

For the first step, we should acquire EHB's plant transfer function from the pressure input to the clamp force exerted on the wheel, which can be derived from Eqs. 5–9. However, using bond graph and equivalent mass (m_{Eq}) and resistance

(b_{Eq}), we can further simplify the equations and the transfer function to a lower degree. The equivalent mass and resistance are defined in the Eqs. 36 and 37 [33].

$$m_{Eq} = m_w + A_w^2 \cdot I_{line} \tag{36}$$

$$b_{Eq} = b_w + A_w^2 \cdot R_{line} \tag{37}$$

The transfer function from the input pressure to the clamp force can be written as (Eq. 38).

$$G_{p_{EHB}} = \frac{F_{cl}}{P_{in}} = \frac{k_{cal} \cdot A_w}{m_{Eq}s^2 + b_{Eq}s + k_{cal}} \tag{38}$$

Since the plant is stable and does not contain any unstable poles or non minimum phase zeros, no interpolation conditions need to be satisfied except selecting a stable Youla transfer function. We have selected this transfer function such that all of the plant's poles are canceled in order to freely shape the closed loop transfer function $T(s)$ and then compute this closed loop transfer function from Eq. 29. We choose the closed loop transfer function to be a second order Butterworth filter (Eq. 40) since this filter shape is optimal and we can freely choose the bandwidth and crossover frequencies. Additionally, we can add a low pass filter to Youla parameter to force it to be small in magnitude at high frequencies as we mentioned in the Section 3.1. This will result in Eqs. 39 and 40. By having T and Y, we can compute the controller using Eqs. 30 and 35. Since this process is the same in all the control designs, from now on, we only calculate Y and T for each loop. The sensitivity transfer function, S, can be computed from T (Eq. 30) and the controller transfer function, (G_c), can be computed using Eq. 35.

$$Y_{EHB} = G_{p_{EHB}}^{-1} \cdot \frac{\omega_n^2}{s^2 + 2\omega_n\xi \cdot s + \omega_n^2} \cdot \frac{W_1}{s + W_1} = \frac{\omega_n^2}{k_{cal} \cdot A_w} \cdot \frac{m_{Eq}s^2 + b_{Eq}s + k_{cal}}{s^2 + 2\omega_n\xi \cdot s + \omega_n^2} \frac{W_1}{s + W_1} \tag{39}$$

$$T_{EHB} = \frac{\omega_n^2}{s^2 + 2\omega_n\xi \cdot s + \omega_n^2} \cdot \frac{W_1}{s + W_1} \tag{40}$$

We now have two control parameters to tune: ω_n, and W_1 (ξ is selected to be $\frac{1}{\sqrt{2}}$ for a second order Butterworth filter). We can choose the natural frequency of the Butterworth filter (ω_n) based on the closed loop bandwidth requirement. In addition, using rule of thumb, we select W_1 to be at least five times bigger that the closed loop bandwidth so that the pole location associated with this transfer function would have no impact on the closed loop bandwidth. **Figure 11** shows a Bode magnitude plot of the T, S and Y based on the proposed control design.

Figure 12 shows the time response of the EHB closed and open loops. The open-loop pressure input is 3.2 kPa (this is chosen to generate the same steady-state results as the closed-loop controller) and the closed-loop is set to follow a 8 kN clamp force target. As shown in **Figure 12**, the controller is capable of following the target well and eliminates the open-loop overshoot.

3.3 EMB Youla control design

Since we have a cascaded control strategy for the EMB actuator, we are required to design three controllers. We start from the inner loop (current control), and the second loop (angular velocity of the shaft), and lastly we make our way up to the most outer loop which is clamp force control.

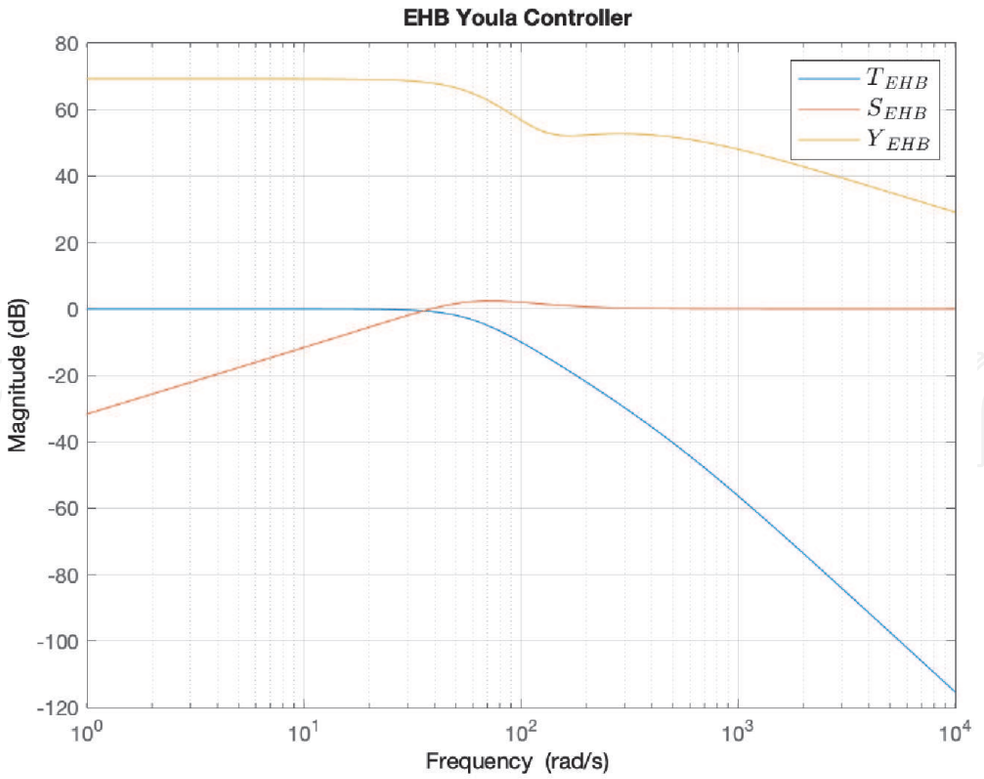

Figure 11.
EHB's designed closed-loop transfer function (T), Youla transfer function (Y), and sensitivity transfer function (S).

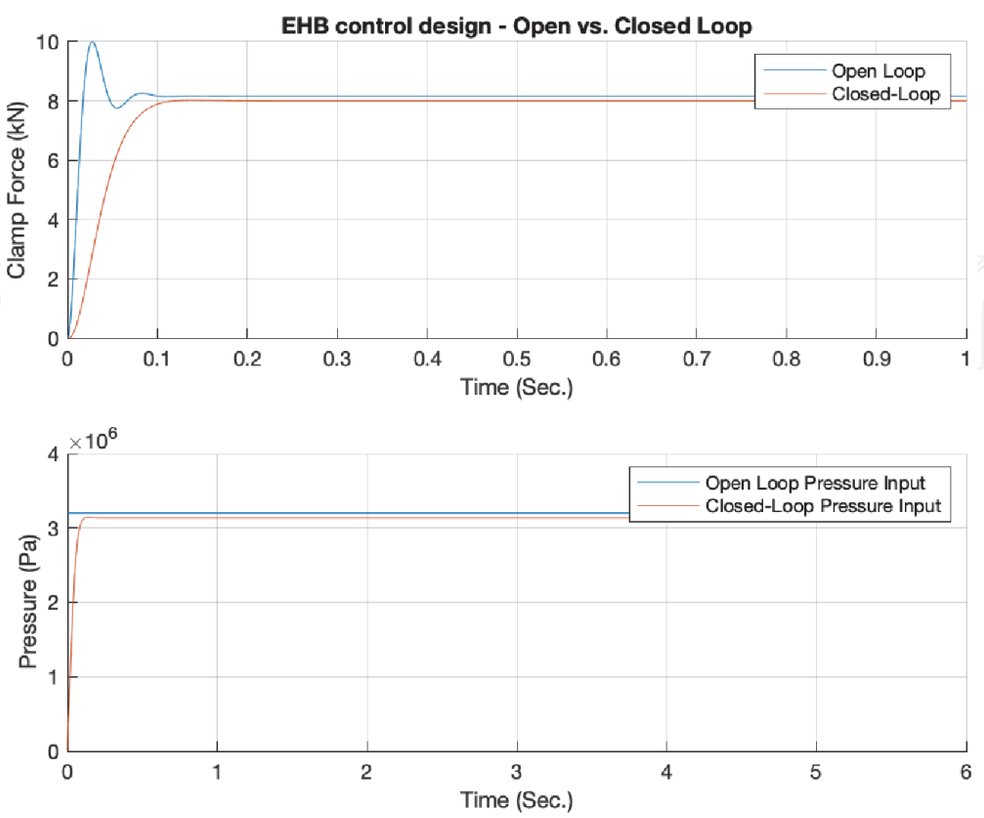

Figure 12.
EHB's controller results - closed loop vs. open loop.

Using Eq. 10, we can calculate the transfer function from the voltage input to the output current. However, we are regarding the last term in the equation $(K_t \cdot \omega_m)$ as a disturbance. The idea is to divide the bond graph into three separate blocks and control each block using the cascaded control strategy. This approach would make the design simpler and more intuitive so that any inputs from other blocks are regarded as disturbances. In this case, the input signal from the gyrator in **Figure 6** is regarded as a disturbance. We can then write the transfer function as Eq. 41.

$$G_{p_{EMB}} = \frac{I_m}{V_{in}} = \frac{\frac{1}{L_m}}{s + \frac{R_m}{L_m}} \tag{41}$$

Since $G_{p_{EMB}}$ has no unstable pole and non-minimum phase zero, we can cancel all the plant poles and create the desired closed loop response. However, canceling all the poles would result in a bigger magnitude of Youla transfer function; therefore, higher actuation effort. Since we want to keep the actuator effort as low as possible, we are going to only use a low-pass filter for Youla transfer function. In this design, we select the Youla transfer function such that the closed loop transfer function T has the same bandwidth as the original plant. The selected Youla transfer function is given by Eq. 42. Based on Y_{EMB_1}, we can compute T_{EMB_1} which is shown in Eq. 43. Another important note, when designing cascaded controllers, is that the closed-loop bandwidth of the inner loop has to be always faster than its outer loop. This ensures that the inner loop follows any command changes of the outer loop and hence, the overall closed loop stability is not compromised.

$$\mathrm{Y}_{EMB_1} = \frac{1}{G_{p_{EMB_1}}(0)} \cdot \frac{W_1}{s + W_1} = R_m \cdot \frac{W_1}{s + W_1} \tag{42}$$

$$T_{EMB_1} = R_m \cdot \frac{W_1}{s + W_1} \cdot \frac{1}{L_m s + R_m} \tag{43}$$

Figure 13a shows that the magnitude of Youla transfer function reduces at high frequency while T and S have their desired shapes.

The controller for the second loop will be designed next. In this case, the new plant to is the inner loop closed-loop transfer function (T_{EMB}) multiplied by the transfer function from the second block open loop related to the dynamics of angular velocity of the shaft. The dynamics of the second block can be derived from Eq. 11 by considering the last term as the disturbance and substituting the nonlinear friction with a linear one $(\tau_f = D_m \cdot \omega_m)$. This results in Eq. 44, and transfer functions Y_{EMB2} and T_{EMB2} are given by Eqs. 45 and 46 respectively.

$$G_{EMB_2} = T_{EMB_1} \cdot \frac{\omega_m}{I_m} = T_{EMB_1} \cdot \frac{\frac{K_t}{J_m}}{s + \frac{D_m}{J_m}} \tag{44}$$

$$\mathrm{Y}_{EMB_2} = \frac{1}{G_{EMB_2}(0)} \cdot \frac{W_2}{s + W_2} = \frac{D_m}{K_t} \cdot \frac{W_2}{s + W_2} \tag{45}$$

$$T_{EMB_2} = D_m \cdot \frac{W_2}{s + W_2} \cdot \frac{W_1}{s + W_1} \cdot \frac{1}{J_m s + D_m} \cdot \frac{R_m}{L_m s + R_m} \tag{46}$$

For the last loop, the transfer function from ω_m to F_{Cl}, the same procedure as the last loop is utilized to compute the open loop transfer function (Eq. 47). As shown in Eq. 47, there is a pole at zero. This pole must be canceled by Youla transfer function to meet the interpolation conditions $(T(0) = 1$ and $S(0) = 0)$, hence,

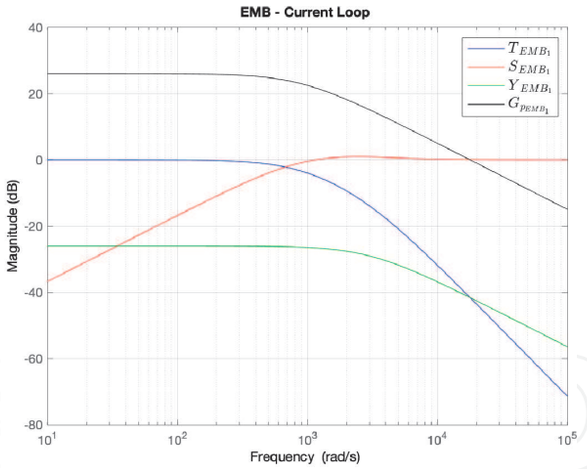

(a)

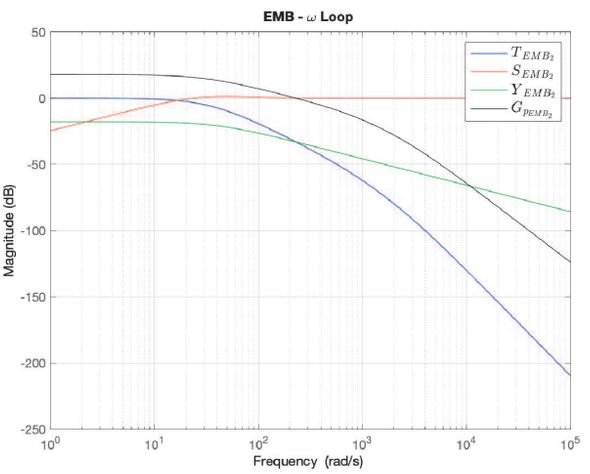

(b)

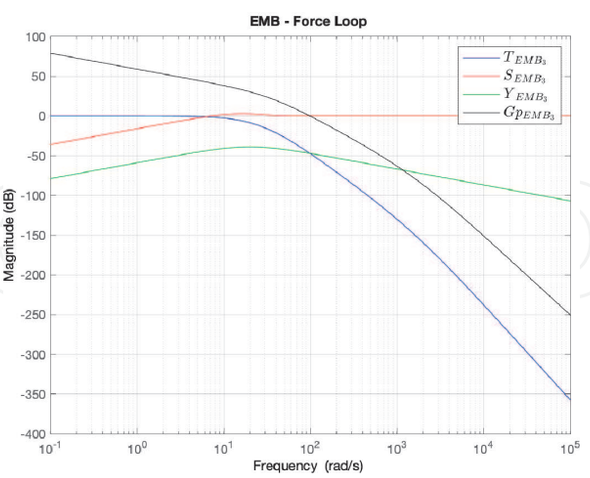

(c)

Figure 13.
EMB's designed closed-loop transfer function (T), Youla transfer function (Y), and sensitivity transfer function (S) for the current, ω and force control loop. (a) Current control bodes, (b) angular velocity control bodes, and (c) force control bodes.

to ensure internal stability. Finally, the transfer functions Y_{EMB2} and T_{EMB2} are given by Eqs. 48 and 49 respectively. The Bode plots are equivalently shown in **Figure 13b** and **c**.

$$G_{EMB_3} = T_{EMB_2} \cdot \frac{F_{cal}}{\omega_m} = T_{EMB_2} \cdot \frac{K_{cal} \cdot N_s \cdot N_p}{s} \tag{47}$$

$$Y_{EMB_3} = \frac{s}{G_{EMB_3} \cdot s(0)} \left(\frac{W_3}{s+W_3}\right)^2 = \frac{s}{K_{cal} \cdot N_s \cdot N_p} \cdot \left(\frac{W_3}{s+W_3}\right)^2 \tag{48}$$

$$T_{EMB_3} = G_{EMB_3} \cdot Y_{EMB_3} = \left(\frac{W_3}{s+W_3}\right)^2 \cdot \frac{W_2}{s+W_2} \cdot \frac{W_1}{s+W_1} \cdot \frac{D_m}{J_m s + D_m} \frac{R_m}{L_m s + R_m} \tag{49}$$

3.4 EWB Youla control design

For this actuator, we follow the same procedure as the EMB and Eqs. 50–58 are the results of this control design process. **Figure 14** shows the magnitude Bode plots of the closed loop transfer functions for the current, angular velocity of the shaft, and clamp force, respectively.

$$G_{p_{EWB_1}} = \frac{I_m}{V_{in}} = \frac{\frac{1}{L_m}}{s + \frac{R_m}{L_m}} \tag{50}$$

$$\mathrm{Y}_{EWB_1} = \frac{1}{G_{p_{EWB_1}}(0)} \cdot \frac{W_1}{s+W_1} = R_m \cdot \frac{W_1}{s+W_1} \tag{51}$$

$$T_{EWB_1} = R_m \cdot \frac{W_1}{s+W_1} \cdot \frac{1}{L_m s + R_m} \tag{52}$$

$$G_{EWB_2} = T_{EWB_1} \cdot \frac{\omega_m}{I_m} = T_{EWB_1} \cdot \frac{\frac{K_t}{J_m}}{s + \frac{D_m}{J_m}} \tag{53}$$

$$Y_{EWB_2} = \frac{1}{G_{EWB_2}(0)} \cdot \frac{W_2}{s+W_2} = \frac{D_m}{K_t} \cdot \frac{W_2}{s+W_2} \tag{54}$$

$$T_{EWB_2} = D_m \frac{W_2}{s+W_2} \frac{W_1}{s+W_1} \frac{1}{J_m s + D_m} \frac{R_m}{L_m s + R_m} \tag{55}$$

$$G_{EWB_3} = T_{EWB_2} \frac{F_{cal}}{\omega_m} = T_{EWB_2} \cdot K_{cal} \cdot \sin(\alpha) \frac{L \cdot N}{2\pi} \cdot \frac{1}{s} \cdot \frac{D_{ax}s + K_{ax}}{m_w s^2 + D_{ax}s + K_{cal} \sin^2\alpha + K_{ax}} \tag{56}$$

$$Y_{EWB_3} = \frac{s}{G_{EWB_3} \cdot s(0)} \cdot \left(\frac{W_3}{s+W_3}\right)^2 = \frac{2\pi \cdot (K_{cal} \cdot \sin^2\alpha + K_{ax})}{K_{cal} \cdot L \cdot N \cdot K_{ax} \sin\alpha} \cdot s \cdot \left(\frac{W_3}{s+W_3}\right)^2 \tag{57}$$

$$\begin{aligned} T_{EWB_3} &= Y_{EWB_3} \cdot G_{EWB_3} \\ &= \left(\frac{W_3}{s+W_3}\right)^2 \frac{W_2}{s+W_2} \frac{W_1}{s+W_1} \cdot \\ &\frac{D_m}{J_m s + D_m} \cdot \frac{R_m}{L_m s + R_m} \cdot \frac{K_{cal} \sin^2\alpha + K_{ax}}{K_{ax}} \cdot \frac{D_{ax}s + K_{ax}}{m_w s^2 + D_{ax}s + K_{cal} \sin^2\alpha + K_{ax}} \end{aligned} \tag{58}$$

3.5 Disturbance rejection

In our previous cascaded control strategy, we ignored the disturbance terms in each loop. However, these disturbance still have a negative impact on each loop's performance. Therefore, we are interested in looking at how each of these

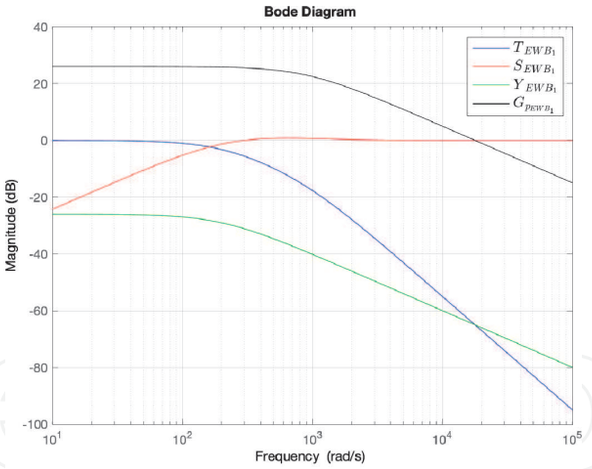

(a)

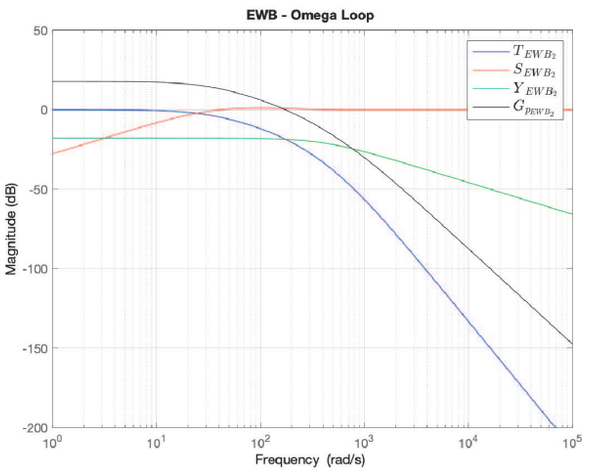

(b)

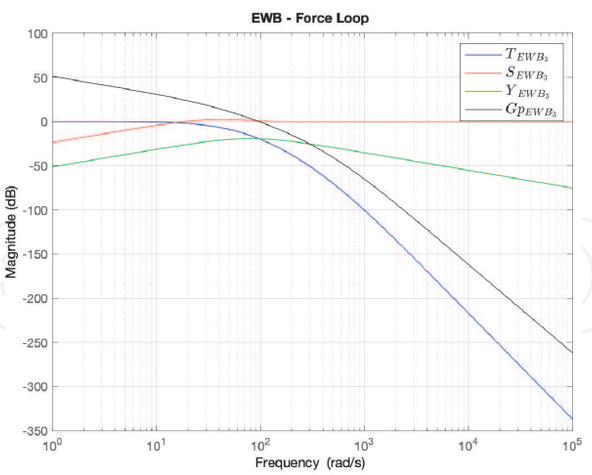

(c)

Figure 14.
EWB's designed closed-loop transfer function (T), Youla transfer function (Y), and sensitivity transfer function (S) for the current, angular velocity of the shaft, and force control loop. (a) Current control bodes, (b) angular velocity control bodes, and (c) force control bodes.

disturbances play a role in the loop. To analyze the effect of disturbances, we need to obtain the disturbance input to the loop output transfer function in each case. This would also help in design a feed-forward disturbance rejection to mitigate the negative effect of disturbances on the output and actuator effort. **Figure 10** shows a

block diagram where the disturbances in the cascaded control loop are given. To mitigate the effect of disturbance in each loop, a feed-forward term is added to reject these disturbances, as shown in **Figure 15**. For the sake of simplicity, the disturbance rejections have not been shown in all the cascaded loops. This disturbance rejection technique can be used wherever the disturbance can be estimated as these disturbance signals cannot be directly measured. Since the estimation might be computationally expensive and not very accurate at times, we should only use disturbance rejection wherever there is a great negative impact on closed loop the performance or on the actuator effort. The effect of the disturbance rejection is shown in Eq. 59 by additional term $-G_{p_d}G_p^{-1}S$

$$u = \left(-G_{p_d} \cdot G_p^{-1}S - Y \cdot G_{p_d}\right) \cdot F_d + Y \cdot r \tag{59}$$

Figure 16 shows the time response of the current loop for a step function of 5 A. As shown, the disturbance rejection has a faster response while maintaining the same level of actuation. It has slightly increases the actuator effort; however, since the closed loop time response with the disturbance rejection is faster, the feedback control loop bandwidth can be reduced to produce the similar time response

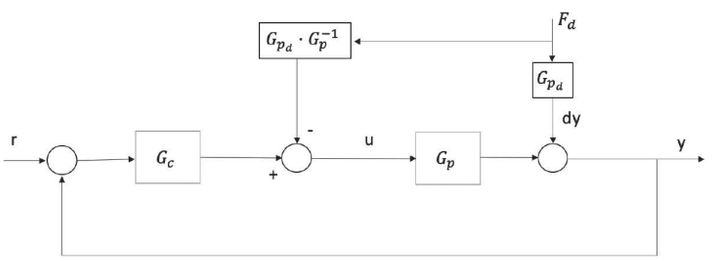

Figure 15.
Block diagram of disturbance rejection scheme used in the cascaded controller loops for EMB/EWB.

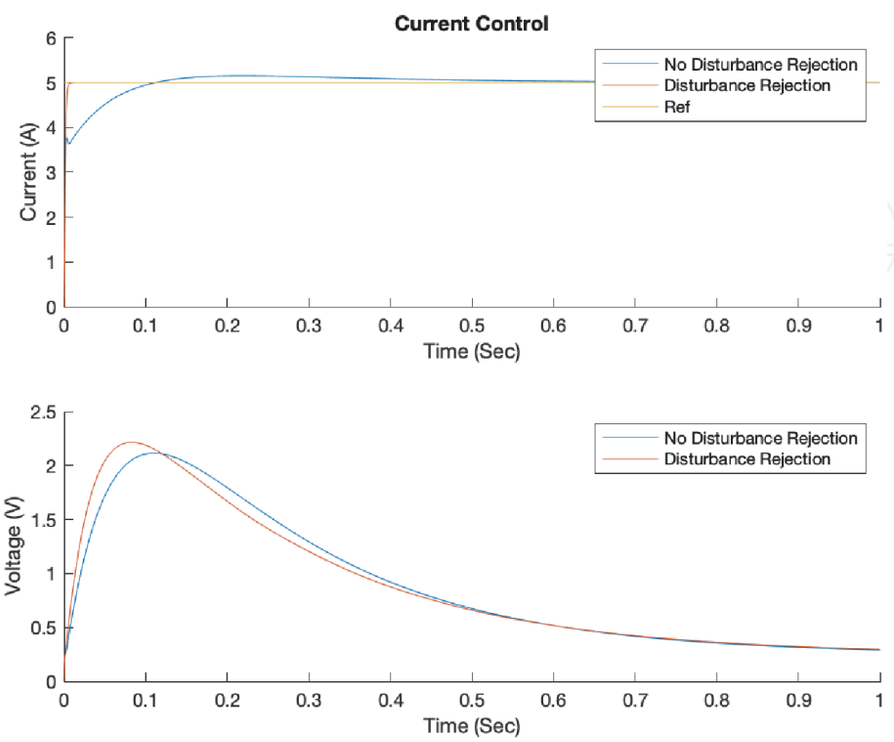

Figure 16.
EMB's current control step time response with and without the disturbance rejection.

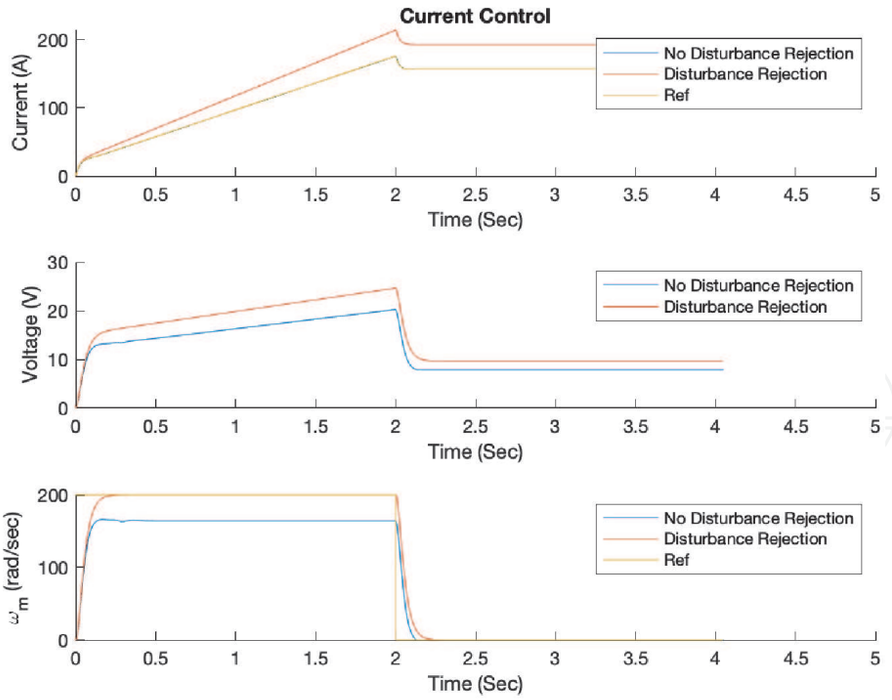

Figure 17.
EMB's angular velocity control pulse response with and without the disturbance rejection.

without the feed-forward term. This way we can reduce the actuation effort. **Figure 17** shows the response of the second loop to a pulse function of 200 $\frac{rad}{sec}$ including the current disturbance rejection capability. This shows that disturbance rejection has a big effect on the steady-state value. Finally, **Figure 18**, shows the result of the actuator's response for a 10-kN clamp force reference. As discussed, when the disturbance rejection scheme is utilized, the closed loop response of the EMB actuator is faster (0.35 seconds vs. 0.8 seconds) while maintaining around the same level of actuation. It should be noted that all the time response simulations are based on nonlinear models. Nonlinearity includes both frictions and actuator

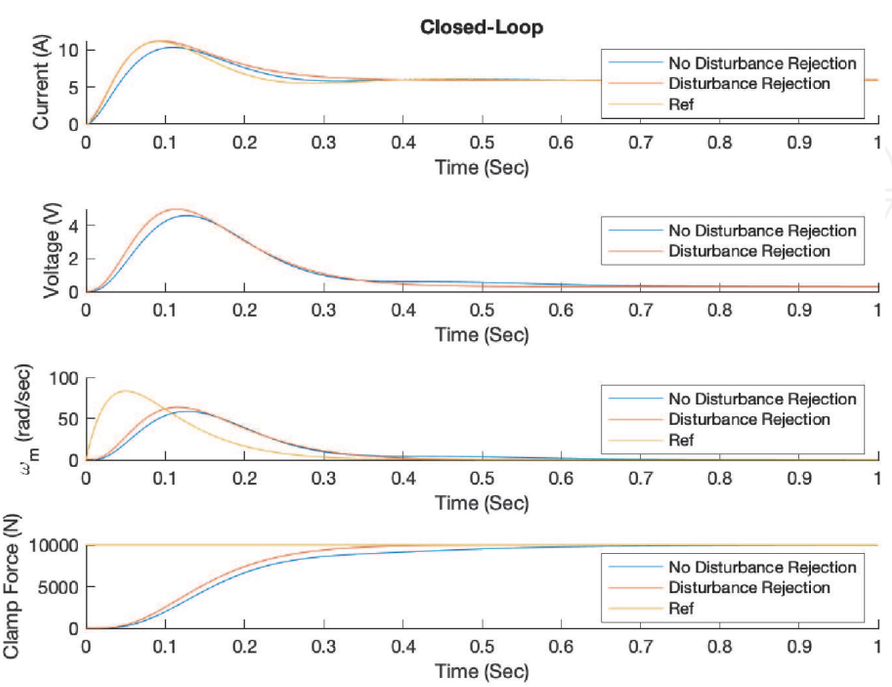

Figure 18.
EMB's closed-loop response over a step function with and without the disturbance rejection.

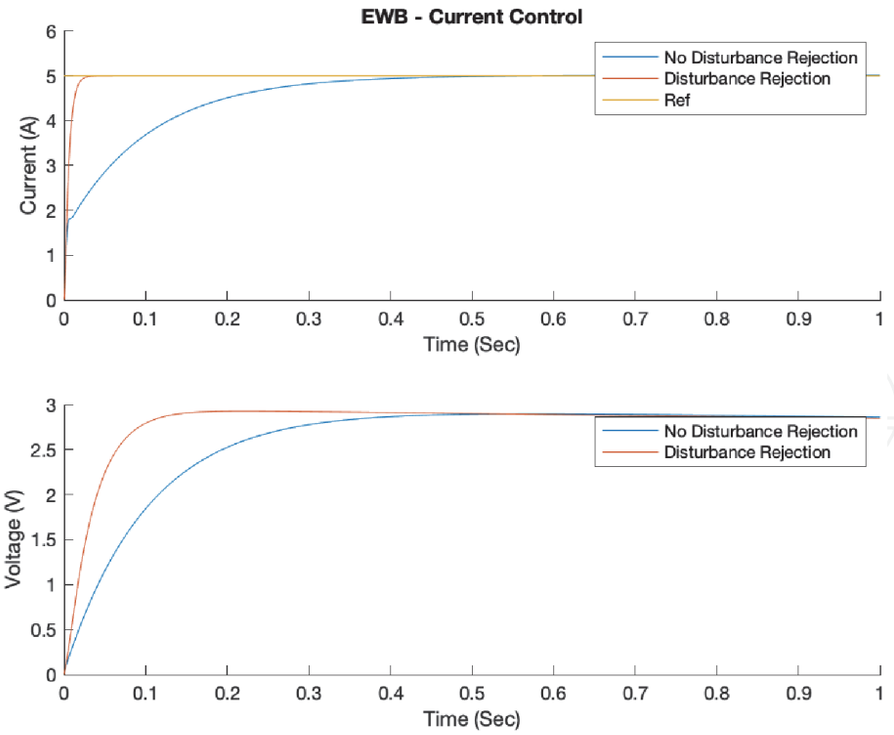

Figure 19.
EWB's current control step time response with and without the disturbance rejection.

saturation limits on the caliper for EMB actuator and only saturation limits for EWB actuator. Future studies will include addition of non-linear frictions to EWB.

Figures 19–21 show the results for the EWB actuator disturbance rejection performances. As shown in **Figure 19**, the disturbance rejection has a great impact on the current control responsiveness while maintaining the same amount of voltage. However, **Figures 20** and **21** show that the second and third loop's disturbance rejections do not have much of impacts on the either closed- loop responses or

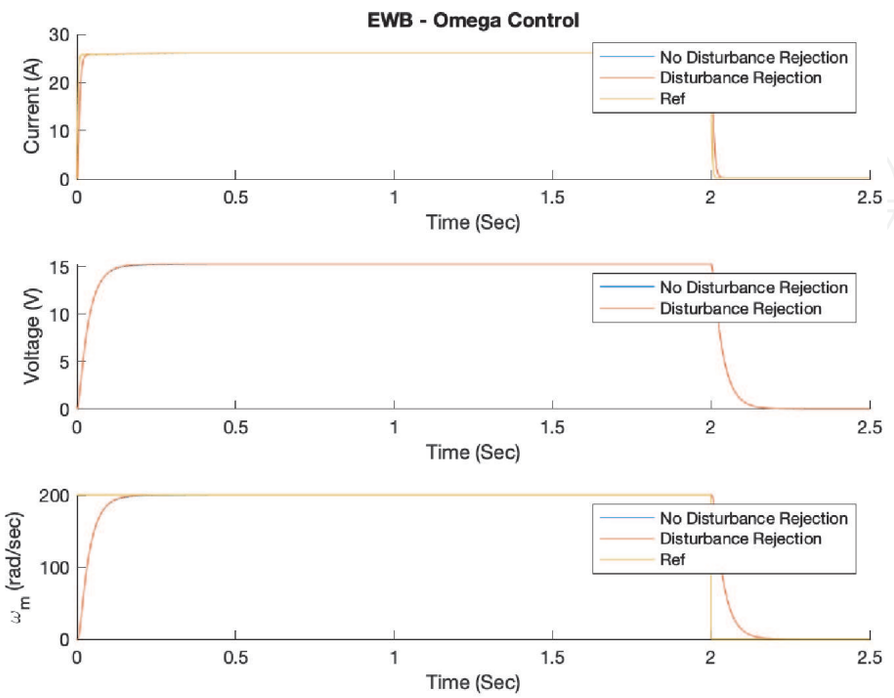

Figure 20.
EWB's angular velocity control pulse response with and without the disturbance rejection.

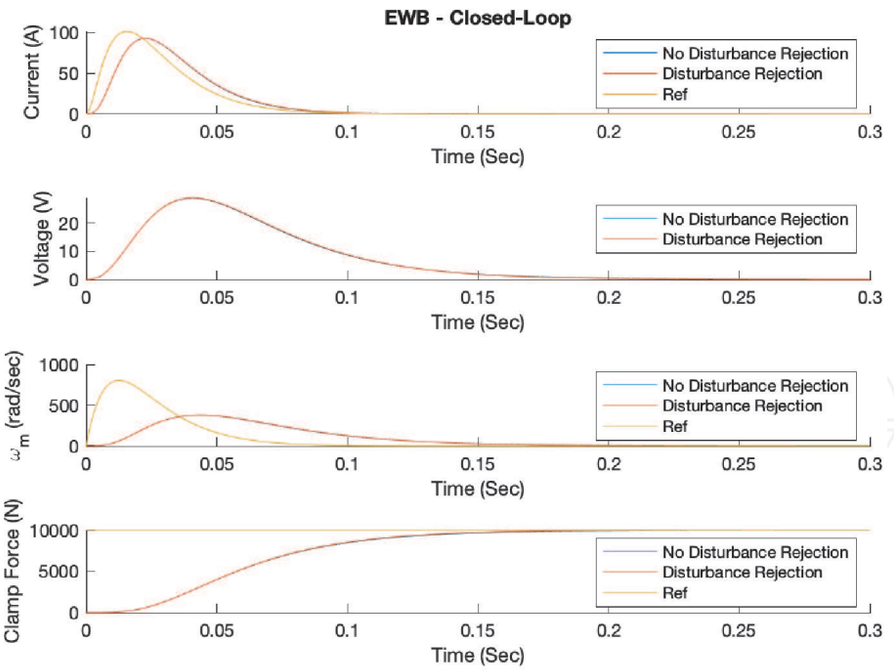

Figure 21.
EWB's closed-loop response over a step function with and without the disturbance rejection.

actuator efforts; therefore, it is recommended, in this case, to only use the current control feedforward disturbance rejection capability and abandon the other disturbance rejections in the second and the third loops.

4. Conclusions

In this chapter, we modeled three different friction brake-by-wire actuators using bond graph method. We then designed closed loop feedback controllers for each actuator using Youla parameterization technique. For the EMB and EWB actuators, we used a cascaded control strategy. Additionally, we designed disturbance rejections for each of their loops. The results of these disturbance rejections were discussed and it was found that EHB has a fastest response compared with the EMB and EWB actuators. However, this comes at higher cost due to addition of hydraulic lines and modules. When comparing the EMB and EWB actuators, based on the given current tuning, EWB has a faster response than the EMB, however, EWB also requires a higher actuator effort. Further investigation is required, by simultaneous optimization of actuators' physical systems including their control parameters, to have a better comparative analysis of the proposed actuators.

Other future studies will include more complex models where additional of some missing physical components (such as hydraulic pump, accumulator, and hydraulic build and dump valves) would be necessary to improve the accuracy of our comparative results. Additionally, a reference trajectory generator can be added, such as [38], to compare the performance of the proposed actuators during an ABS maneuver.

Acknowledgements

Authors would like to thank Louis Filipozzi and Kevin R. Mallon for their comments and review of this book chapter.

DOI: http://dx.doi.org/10.5772/intechopen.94581

Author details

Ehsan Arasteh* and Francis Assadian
University of California, Davis, USA

*Address all correspondence to: earasteh@ucdavis.edu

References

[1] Yuan Y, Zhang J, Li Y, Lv C. Regenerative Brake-by-Wire System Development and Hardware-in-Loop Test for Autonomous Electrified Vehicle. Available from: https://www.sae.org/content/2017-01-0401/.

[2] Sinha P. Architectural Design and Reliability Analysis of a Fail-Operational Brake-by-Wire System from ISO 26262 Perspectives;96(10):1349–1359. Available from: https://linkinghub.elsevier.com/retrieve/pii/S095183201100041X.

[3] Gombert BDM, Schautt M, Roberts RP. The Development of Alternative Brake Systems. In: Crolla D, Foster DE, Kobayashi T, Vaughan N, editors. Encyclopedia of Automotive Engineering. John Wiley & Sons, Ltd;. p. 1–11. Available from: http://doi.wiley.com/10.1002/9781118354179.auto025.

[4] Bob Chabot. Brake to the Future; pp. 18–24. Available from: https://www.motor.com/magazine-summary/brake-to-the-future.

[5] Hofmann D, Binder J, Pfau M, Schunck E. Hydraulic brake system for a vehicle. Google Patents; 2000. US Patent 6,149,247.

[6] Feigel HJ. Integrated Brake System without Compromises in Functionality; 114(7–8):46–50. Available from: http://link.springer.com/10.1007/s38311-012-0192-y.

[7] Cheon JS. Brake By Wire System Configuration and Functions Using Front EWB (Electric Wedge Brake) and Rear EMB (Electro-Mechanical Brake) Actuators;. Available from: https://www.sae.org/content/2010-01-1708/.

[8] Line C, Manzie C, Good M. Control of an Electromechanical Brake for Automotive Brake-By-Wire Systems with an Adapted Motion Control Architecture;. Available from: http://papers.sae.org/2004-01-2050/.

[9] Yamasaki T, Eguchi M, Makino Y. Development of an Electromechanical Brake; p. 9.

[10] Line C, Manzie C, Good MC. Electromechanical Brake Modeling and Control: From PI to MPC;16(3):446–457. Available from: http://ieeexplore.ieee.org/document/4475522/.

[11] Schwarz R, Isermann R, Böhm J, Nell J, Rieth P. Modeling and Control of an Electromechanical Disk Brake;. Available from: http://papers.sae.org/980600/.

[12] Line C, Manzie C, Good M. ROBUST CONTROL OF AN AUTOMOTIVE ELECTROMECHANICAL BRAKE;40(10):579–586. Available from: https://linkinghub.elsevier.com/retrieve/pii/S1474667015319765.

[13] Sakamoto T, Hirukawa K, Ohmae T. Cooperative Control of Full Electric Braking System with Independently Driven Four Wheels. In: 9th IEEE International Workshop on Advanced Motion Control, 2006. IEEE;. p. 602–606. Available from: http://ieeexplore.ieee.org/document/1631728/.

[14] Hartmann H, Schautt M, Pascucci A, Gombert B. eBrake® - The Mechatronic Wedge Brake;. p. 2002–01–2582. Available from: https://www.sae.org/content/2002-01-2582/.

[15] Fox J, Roberts R, Baier-Welt C, Ho LM, Lacraru L, Gombert B. Modeling and Control of a Single Motor Electronic Wedge Brake;. Available from: https://www.sae.org/content/2007-01-0866/.

[16] Han K, Kim M, Huh K. Modeling and Control of an Electronic Wedge

Brake;226(10):2440–2455. Available from: http://journals.sagepub.com/doi/10.1177/0954406211435584.

[17] Che Hasan MH, Khair Hassan M, Ahmad F, Marhaban MH. Modelling and Design of Optimized Electronic Wedge Brake. In: 2019 IEEE International Conference on Automatic Control and Intelligent Systems (I2CACIS). IEEE;. p. 189–193. Available from: https://ieeexplore.ieee.org/document/8825045/.

[18] Cheon JS, Kim J, Jeon J. New Brake By Wire Concept with Mechanical Backup;5(4):1194–1198. Available from: https://www.sae.org/content/2012-01-1800/.

[19] Emam MAA, Emam AS, El-Demerdash SM, Shaban SM, Mahmoud MA. Performance of Automotive Self Reinforcement Brake System;1(1):7.

[20] Ahmad F, Hudha K, Mazlan S, Jamaluddin H, Aparow V, Yunos MM. Simulation and Experimental Investigation of Vehicle Braking System Employing a Fixed Caliper Based Electronic Wedge Brake;94(4):327–340. Available from: http://journals.sagepub.com/doi/10.1177/0037549717733805.

[21] Ho LM, Roberts R, Hartmann H, Gombert B. The Electronic Wedge Brake - EWB;. Available from: https://www.sae.org/content/2006-01-3196/.

[22] Putz MH, Wunsch C, Morgan J, Schiffer M, Brugger J. Energy and Timing Advantages of Highly Non-Linear EMB Actuation;. Available from: https://www.sae.org/content/2013-01-2067/.

[23] Putz MH, Wunsch C, Schiffer M, Peternel J. Test Results of A Sensor-Less, Highly Nonlinear Electro-Mechanical Brake;. Available from: https://www.sae.org/content/2014-01-2541/.

[24] Putz MH, Wunsch C, Morgan J. The VE Electro-Mechanical Car Brake for Windmills (and Railways);. Available from: https://www.sae.org/content/2012-01-1796/.

[25] Putz MH. VE Mechatronic Brake: Development and Investigations of a Simple Electro Mechanical Brake;. Available from: https://www.sae.org/content/2010-01-1682/.

[26] Karnopp D, Margolis DL, Rosenberg RC. System Dynamics: Modeling and Simulation of Mechatronic Systems. 5th ed. Wiley;.

[27] Yi J, Alvarez L, Horowitz R, de Wit CC. Adaptive Emergency Braking Control Using a Dynamic Tire/Road Friction Model. In: Proceedings of the 39th IEEE Conference on Decision and Control (Cat. No.00CH37187). vol. 1. IEEE;. p. 456–461. Available from: http://ieeexplore.ieee.org/document/912806/.

[28] Anwar S. An Anti-Lock Braking Control System for a Hybrid Electromagnetic/Electrohydraulic Brake-by-Wire System. In: Proceedings of the 2004 American Control Conference. IEEE;. p. 2699–2704 vol.3. Available from: https://ieeexplore.ieee.org/document/1383873/.

[29] Loyola J, Assadian F. An Investigation Into New ABS Control Strategies;9(2):869–876. Available from: https://www.sae.org/content/2016-01-1639/.

[30] Filipozzi L, Assadian F, Kuang M, Johri R, Alcantar JV. An Investigation into the Traction and Anti-Lock Braking System Control Design. In: SAE Technical Paper. SAE International; 2020. Available from: https://doi.org/10.4271/2020-01-0997.

[31] Burckhardt, Manfred. Fahrwerktechnik: Radschlupf-Regelsysteme. Vogel-Verlag, Wurtzburg.

[32] Canudas de Wit C, Horowitz R, Tsiotras P. Model-Based Observers for

Tire/Road Contact Friction Prediction. In: Nijmeijer H, Fossen TI, editors. New Directions in Nonlinear Observer Design. vol. 244 of Lecture Notes in Control and Information Sciences. Springer London;. p. 23–42. Available from: http://link.springer.com/10.1007/BFb0109919.

[33] Loyola J. An investigation into new ABS control strategies; 2017.

[34] Wang N, A Kaganov aAK S Code. Actuating Mechanism and Brake Assembly [patent;](WO 2005/124180 A1):13.

[35] Ahn JK, Jung KH, Kim DH, Jin HB, Kim HS, Hwang SH. Analysis of a Regenerative Braking System for Hybrid Electric Vehicles Using an Electro-Mechanical Brake;10(2):229–234. Available from: http://link.springer.com/10.1007/s12239-009-0027-z.

[36] Karnopp D. Computer Simulation of Stick-Slip Friction in Mechanical Dynamic Systems;107(1):100–103. Available from: https://asmedigitalcollection.asme.org/dynamicsystems/article/107/1/100/400601/Computer-Simulation-of-StickSlip-Friction-in.

[37] Assadian F, Mallon K. Robust Control: Youla Parameterization Approach. JOHN WILEY; 2020.

[38] Arasteh E, Assadian F, Filipozzi L. Algorithm to Generate Target for Anti-Lock Braking System Using Wheel Power;2:6.